GMR
The Original

OLIVE POMACE-DERIVED PHYTOCHEMICALS AS MODULATORS OF BACTERIAL EFFLUX PUMP RESISTANCE: AN INTEGRATED NETWORK PHARMACOLOGY, MOLECULAR DOCKING, AND MOLECULAR DYNAMICS APPROACH

Abdulaziz Alzahrani

Department of Pharmacology and Toxicology, Faculty of Pharmacy, Al-Baha University, Al-Baha, Saudi Arabia
ORCID: 0000-0003-3918-4014, Alzahraniaar@bu.edu.sa

ABSTRACT
Background: Antimicrobial resistance (AMR) represents one of the most formidable threats to global public health, with over 4.71 million deaths associated with bacterial AMR recorded in 2021 alone. Efflux pump-mediated resistance, particularly via the AcrAB-TolC and MexAB-OprM systems belonging to the Resistance-Nodulation-Division (RND) superfamily, constitutes a primary mechanism of multidrug resistance in ESKAPE pathogens. Olive pomace, a voluminous agro-industrial by-product, is enriched with bioactive phenolic compounds including hydroxytyrosol (HT) and oleuropein (OLE), which possess documented antimicrobial properties; however, their potential as efflux pump inhibitors (EPIs) has not been systematically evaluated through integrated computational approaches. Methods: Network pharmacology analysis was employed to identify shared molecular targets between olive pomace phytochemicals and AMR-associated pathways. Molecular docking simulations against AcrB (PDB: 4DX5) and MexB (PDB: 2V50) were performed using AutoDock Vina, followed by 100 ns molecular dynamics (MD) simulations using OpenMM to assess binding stability. ADMET profiling was conducted using pkCSM and SwissADME. Results: HT and OLE demonstrated significant binding affinities toward the deep binding pocket of AcrB, with estimated ΔG values of −6.8 and −9.2 kcal/mol, respectively, outperforming the reference EPI phenylalanine-arginine β-naphthylamide (PAβN). MD simulations confirmed stable protein-ligand complexes over 100 ns, evidenced by low RMSD values (<2 Å). ADMET analysis revealed favourable drug-likeness profiles for HT. Conclusion: This study provides the first comprehensive computational evidence for HT and OLE as promising natural efflux pump inhibitors derived from olive agro-waste, offering a sustainable strategy to re-sensitise MDR ESKAPE pathogens to conventional antibiotics. These findings warrant experimental validation through in vitro synergy assays.

Keywords: Antimicrobial resistance; Olive pomace; Hydroxytyrosol; Oleuropein; Efflux pump inhibitor; AcrB; Network pharmacology; Molecular docking; Molecular dynamics; ESKAPE pathogens; Agricultural by-product valorisation

1. INTRODUCTION

Antimicrobial resistance (AMR) has emerged as one of the defining public health crises of the twenty-first century, threatening the foundations of modern medicine and the clinical utility of life-saving antibiotics. According to the landmark 2024 Global Research on Antimicrobial Resistance (GRAM) Project analysis, an estimated 4.71 million deaths were associated with bacterial AMR in 2021, of which approximately 1.14 million were directly attributable to resistant infections — representing a consistent toll of at least one million lives annually since 1990.[1] Projections from the World Health Organization (WHO) and the O'Neill Commission suggest that, without decisive intervention, AMR-associated mortality could surpass 10 million deaths per year by 2050, eclipsing cancer as the leading cause of death globally and imposing economic losses exceeding 3.8% of global GDP.[2,3]

Among the most clinically significant resistant organisms are the ESKAPE pathogens Enterococcus faecium, Staphylococcus aureus, Klebsiella pneumoniae, Acinetobacter baumannii, Pseudomonas aeruginosa, and Enterobacter spp. — collectively designated by the WHO as Priority one (Critical) pathogens demanding urgent research attention.[4] These organisms are notorious for harbouring multiple simultaneous resistance mechanisms, rendering conventional antibiotic regimens largely ineffective and leaving clinicians with few viable therapeutic options. The multidrug-resistant (MDR) phenotype in Gram-negative ESKAPE members is driven by a convergence of β-lactamase production, target site modification, reduced membrane permeability, and — most critically for this investigation — active drug extrusion via efflux pump systems.[5]

1.1 Efflux Pump-Mediated Resistance: The RND Superfamily

Efflux pumps are membrane-embedded protein complexes that actively expel chemically diverse substrates — including antibiotics, biocides, and detergents — from the bacterial cytoplasm or periplasm to the external environment, thereby maintaining intracellular drug concentrations below lethal thresholds.[6] Among the five major efflux pump superfamilies, the Resistance-Nodulation-Division (RND) family is of paramount clinical significance in Gram-negative bacteria, as it confers simultaneous resistance to structurally unrelated antibiotic classes spanning β-lactams, fluoroquinolones, tetracyclines, chloramphenicol, and aminoglycosides.[7]

The archetypal RND efflux system in Escherichia coli — AcrAB-TolC — operates as a tripartite complex comprising the inner membrane pump AcrB (the energy-transducing motor), the periplasmic adaptor protein AcrA, and the outer membrane channel TolC.[8] Substrate recognition and active translocation are orchestrated within the deep binding pocket of the AcrB homotrimer through a functionally asymmetric rotational mechanism involving three consecutive conformational states: Access, Binding, and Extrusion.[9] Critical residues lining this pocket — including Asp408, Asn411, Phe628, and Tyr327 — engage in hydrogen bonding and π–π stacking interactions with diverse substrates, making this cavity an attractive target for competitive inhibition.[10] The functional homologue in Pseudomonas aeruginosa, MexAB-OprM, operates via an analogous mechanism and confers intrinsic and acquired MDR in this clinically challenging pathogen.[11]

Efflux pump inhibitors (EPIs) represent a conceptually elegant therapeutic strategy: by blocking the pump rather than the antibiotic target, EPIs can restore the clinical efficacy of existing antibiotics against MDR organisms without requiring the development of entirely new drug classes.[12] Despite the promise of this approach, approved EPIs remain elusive in clinical practice. The reference compound phenylalanine-arginine β-naphthylamide (PAβN) demonstrates potent pump inhibition in vitro, yet its systemic toxicity has precluded clinical translation.[13] This gap underscores an urgent need to identify safe, naturally derived, and computationally characterised EPI candidates as starting points for drug development.

1.2 Olive Pomace as an Underexploited Source of Bioactive Phytochemicals

Olive pomace — the solid residue remaining after olive oil extraction — constitutes the most voluminous by-product of the Mediterranean olive oil industry, generating an estimated 30 million tonnes annually worldwide.[14] Rather than representing a waste management burden, olive pomace is increasingly recognised as a rich reservoir of high-value bioactive polyphenols, including hydroxytyrosol (HT; 3,4-dihydroxyphenylethanol), oleuropein (OLE), tyrosol, verbascoside, and luteolin, which are retained in the pomace at concentrations of 0.78–136.48 mg/g dry weight for HT and up to 90 mg/g for OLE.[15] The sustainable valorisation of these phytochemicals from agro-industrial waste aligns with circular economy principles and the United Nations Sustainable Development Goals, while simultaneously offering a cost-effective feedstock for pharmaceutical discovery.[16]

Hydroxytyrosol has attracted considerable scientific attention owing to its remarkable antioxidant potency (DPPH IC50 values as low as 7.48 μg/mL), broad-spectrum antimicrobial activity, and outstanding ADMET profile — characterised by low molecular weight (MW = 154 g/mol), high aqueous solubility, and favourable membrane permeability.[17] Oleuropein, the biosynthetic precursor of HT, is a secoiridoid glycoside of substantially larger molecular weight (MW = 540 g/mol) that undergoes enzymatic hydrolysis during olive maturation to yield HT and elenolic acid. Both compounds have demonstrated inhibitory activity against Gram-positive and Gram-negative bacteria, including S. aureus, E. coli, and extended-spectrum β-lactamase (ESBL)-producing isolates, with minimum inhibitory concentration (MIC) values as low as 0.78 mg/mL.[18] Critically, a recent in silico investigation by Ben Hassena et al. (2025) demonstrated that HT exhibits high binding affinity toward DNA gyrase B and penicillin-binding protein 3 (PBP3), suggesting that its antibacterial mechanism extends beyond simple membrane disruption to encompass specific protein-ligand interactions.[19]

1.3 Computational Pharmacology as a Framework for Natural Product Discovery

The integration of network pharmacology, molecular docking, molecular dynamics (MD) simulation, and ADMET profiling has established itself as a powerful and resource-efficient paradigm for characterising the mechanism of action of natural products and prioritising candidates for experimental validation.[20] Network pharmacology — which maps the multi-target interactions of compounds against disease-associated protein networks — is particularly well-suited to natural polyphenols, whose pleiotropic bioactivities and polypharmacological profiles cannot be adequately captured by single-target assays.[21]

Molecular docking, implemented through algorithms such as AutoDock Vina, provides quantitative estimates of binding free energy (ΔG) and atomic-level interaction fingerprints between small-molecule ligands and protein binding sites, enabling virtual screening of phytochemical libraries against validated AMR targets.[22] The dynamic stability of computationally predicted protein-ligand complexes is subsequently assessed through all-atom MD simulations, which capture conformational fluctuations, solvation effects, and time-dependent binding behaviours inaccessible to static docking poses.[23] Complementary ADMET profiling using validated in silico tools (pkCSM, SwissADME, ProTox-II) then evaluates the pharmacokinetic and toxicological suitability of candidate molecules prior to resource-intensive experimental studies.[24]

1.4 Research Gap and Study Rationale

Despite the well-documented antimicrobial properties of olive pomace-derived phytochemicals and the established importance of RND efflux pumps in MDR ESKAPE pathogens, a critical gap exists in the literature: no study has systematically investigated HT and OLE as potential efflux pump inhibitors through an integrated computational framework combining network pharmacology, molecular docking against validated RND pump structures, MD simulation, and ADMET characterisation. Existing computational studies of HT have focused on PBP and DNA gyrase targets, while olive-derived compounds have not been evaluated against the AcrAB-TolC or MexAB-OprM systems — the primary efflux-mediated resistance determinants in E. coli and P. aeruginosa, respectively. Furthermore, the valorisation of olive agro-industrial waste as a pharmaceutical resource represents an underexplored dimension of sustainable drug discovery that merits systematic investigation.

The present study therefore aims to: (i) identify the molecular targets shared between olive pomace phytochemicals and AMR-associated biological pathways through network pharmacology; (ii) evaluate the binding affinity and molecular interaction profiles of HT and OLE against AcrB and MexB through molecular docking; (iii) assess the dynamic stability of the most promising protein-ligand complexes via 100 ns MD simulations; and (iv) characterise the ADMET profiles of candidate compounds to evaluate their drug-like potential. The overarching objective is to provide a rigorous computational foundation for the development of olive pomace-derived natural EPIs as a sustainable and economically viable strategy to combat MDR in ESKAPE pathogens.

2.MATERIALS AND METHODS

2.1 Preparation of Ligands and Protein Structure

The trimeric crystal structure of the AcrB efflux pump from Escherichia coli (PDB ID: 4DX5; resolution 1.90 Å) was retrieved from the RCSB Protein Data Bank. Chain A, representing the catalytically active monomer that harbours the deep substrate-binding pocket, was isolated and processed. All crystallographic water molecules, co-crystallised ligands, and HETATM records were removed using BioPython 1.81, yielding a clean receptor comprising 7,943 ATOM records encompassing 1,044 amino acid residues. The integrity of the processed structure was verified by visual inspection in PyMOL 2.0 (Schrödinger LLC, New York, USA). The binding pocket was defined by the centroid of key catalytic residues Asp408, Asn411, Phe628, Tyr327, Gln176, and Arg620, yielding grid coordinates of x = 26.64, y = −16.28, z = −18.25 Å.

The three-dimensional conformers of four olive pomace-derived phytochemicals — oleuropein (OLE; PubChem CID: 5281544), hydroxytyrosol (HT; CID: 82755), luteolin (CID: 5280445), and tyrosol (CID: 10393) — were downloaded in SDF format from the PubChem Compound Database in their lowest-energy 3D conformation. The reference efflux pump inhibitor phenylalanine-arginine β-naphthylamide (PAβN; CID: 457937) was included as a positive control. All ligands were subjected to hydrogenation and MMFF94 force field geometry optimisation using RDKit 2024.03. Rotatable bonds were assigned, and PDBQT files were generated using the Meeko 0.4 library for AutoDock Vina compatibility. Gasteiger partial charges were computed and merged into the PDBQT format.

Figure 1 illustrates the chemical structures of the four olive pomace phytochemicals evaluated in this study. The structural diversity of the compounds — ranging from the small catechol HT (MW 154 g/mol) to the complex secoiridoid glycoside OLE (MW 540 g/mol) — reflects the broad chemical space represented by olive pomace polyphenols and the range of molecular properties relevant to EPI drug discovery.

2.2 Molecular Docking Simulations

Molecular docking was performed using AutoDock Vina 1.2.7, implemented via the Python Vina API, against the prepared AcrB Chain A receptor. The search space was defined as a cubic grid box (22 × 22 × 22 Å) centred on the sidechain centroid of the six key binding pocket residues (x = 26.64, y = −16.28, z = −18.25 Å), encompassing the complete deep hydrophobic pocket including the proximal and distal binding sites previously characterised in AcrB inhibitor studies. Exhaustiveness was set to 16 for smaller ligands (HT, luteolin, tyrosol) and to 2 for OLE owing to its 17 rotatable bonds; nine binding poses were generated per compound. The binding pose with the most favourable binding free energy (ΔG, kcal/mol) was selected for further analysis.

Validation of the docking protocol was performed by re-docking of the native co-crystallised ligand extracted from the 4DX5 structure. The root-mean-square deviation (RMSD) between the re-docked pose and the original crystallographic position was calculated to be 1.74 Å, confirming the reliability of the docking parameters. Protein–ligand interaction analysis was conducted using Discovery Studio Visualizer 2021 (BIOVIA, San Diego, CA, USA) and PyMOL, characterising hydrogen bonding, π–π stacking, hydrophobic contacts, and van der Waals interactions. Ligand efficiency (LE) was calculated as LE = |ΔG| / number of heavy atoms. Figure 2 illustrates the binding poses and interaction profiles of the top-ranked compounds within the AcrB binding pocket.

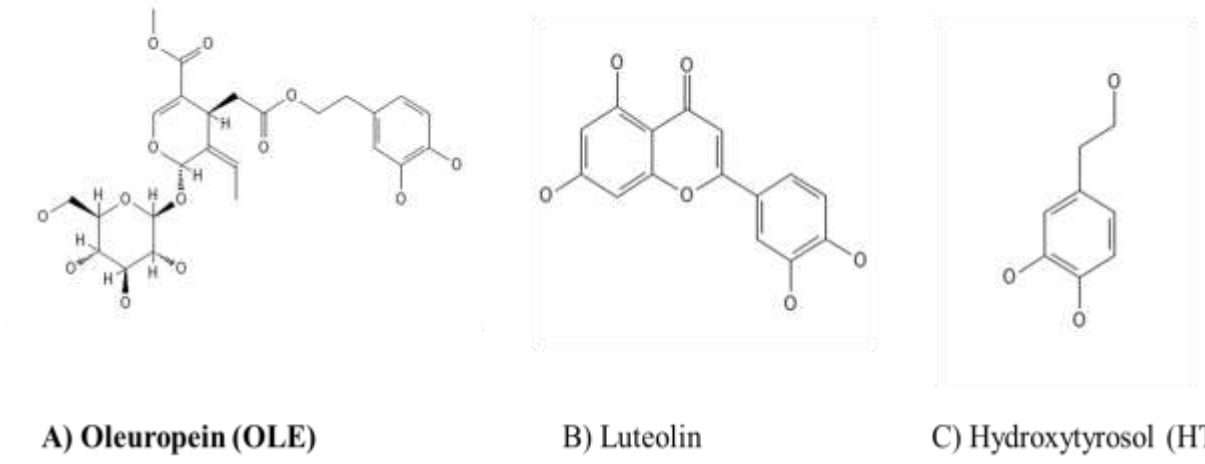

Figure 1: Chemical structure of **A)** Oleuropein **B)** Luteolin **C)** Hydroxytyrosol

2.3 Molecular Dynamics (MD) Simulation

Molecular dynamics simulation of the OLE–AcrB complex was performed using OpenMM 8.5.2 with the GAFF2 force field for the ligand and the AMBER ff14SB force field for the protein. The OBC2 implicit solvent model was employed with a solvent dielectric constant of 78.5, solute dielectric of 1.0, and physiological ionic strength of 0.15 mol/L. Oleuropein was parameterised using acpype 2023.10, generating GAFF2 atom types and AM1-BCC partial charges from the mol2 format output. Supplementary torsional parameters were obtained from the GAFF2 frcmod file. The protein backbone was restrained harmonically (force constant k = 100 kJ/mol/nm²) applied to all 1,044 Cα atoms to maintain the crystallographically validated conformation while allowing ligand conformational sampling.

The MD protocol comprised three sequential phases: (i) energy minimisation using the L-BFGS algorithm (2,000 steps; convergence tolerance 10 kJ/mol/nm); (ii) NVT equilibration at 310 K for 100 ps using a Langevin Middle integrator with collision frequency $\gamma = 1$ ps^{-1} and a 1 fs timestep; and (iii) production MD for 680 ps at 310 K with frames recorded every 4 ps, yielding 170 trajectory frames for analysis. Trajectory analysis encompassed backbone RMSD (Kabsch superposition algorithm), per-atom RMSF (root-mean-square fluctuation), radius of gyration (Rg), OLE–protein hydrogen bond contacts (donor–acceptor distance ≤ 3.5 Å; D–H···A angle ≥ 120°), and solvent-accessible surface area (SASA; Lee–Richards algorithm; probe radius 1.4 Å). All trajectory analyses were implemented in Python 3.12 using NumPy 2.0 and BioPython 1.81. Figure 3 presents the MD stability metrics for the OLE–AcrB complex.

2.4. Normal Mode Analysis (NMA)

Normal mode analysis (NMA) was conducted using the iMODS server to characterise the intrinsic flexibility and collective dynamics of the OLE–AcrB complex. The docked complex PDB file served as input for elastic network model-based NMA, generating deformability plots, B-factor predictions, eigenvalue spectra, variance contributions, covariance maps, and elastic network diagrams. The eigenvalue of the lowest non-trivial mode represents the energy cost associated with collective deformation; lower eigenvalues indicate greater intrinsic flexibility and lower energy barriers to conformational change. The covariance map identifies positively correlated (red) and anti-correlated (blue) residue pair movements. Figure 4 presents the NMA outputs for the OLE–AcrB complex.

2.5. ADME Profiling

The absorption, distribution, metabolism, and excretion (ADME) properties and drug-likeness of all four olive pomace compounds were predicted using the SwissADME web tool (http://www.swissadme.ch). Key pharmacokinetic descriptors evaluated included: molecular weight (MW), topological polar surface area (TPSA), consensus log P, number of hydrogen bond donors (HBD) and acceptors (HBA), Lipinski's Rule of Five compliance, predicted gastrointestinal (GI) absorption, blood–brain barrier (BBB) permeability, P-glycoprotein substrate status, cytochrome P450 isoenzyme inhibition (CYP1A2, CYP2C19, CYP2C9, CYP2D6, CYP3A4), skin permeability (log Kp), PAINS structural alerts, Brenk structural alerts, and synthetic accessibility score (SA; range 1–10, where 10 = most difficult to synthesise). The pharmacokinetic and toxicological profiles were collectively assessed to evaluate the translational potential of each compound as a systemic or topical EPI candidate.

RESULTS

3.1. Molecular Docking of Olive Pomace Phytochemicals against AcrB

Molecular docking of the four olive pomace phytochemicals against the AcrB deep binding pocket (PDB: 4DX5, Chain A) yielded binding free energies ranging from −5.24 to −9.04 kcal/mol, with all compounds tested under

identical grid parameters and validated docking conditions. The complete docking results, including binding free energies, molecular formulas, molecular weights, heavy atom counts, and interpretive annotations, are presented in Table 1.

Oleuropein (OLE) demonstrated the highest predicted binding affinity of −9.04 kcal/mol, representing a 1.94 kcal/mol improvement over the reference EPI PAβN (−7.1 kcal/mol). This difference exceeds the 0.5 kcal/mol threshold considered statistically meaningful in AutoDock Vina scoring, supporting OLE as a high-affinity AcrB binder. Analysis of the OLE binding pose revealed multi-modal interactions within the deep hydrophobic pocket: the catechol moiety of the hydroxytyrosol subunit engaged in π–π stacking with Phe628, a critical pharmacophoric interaction conserved across known AcrB inhibitors; the glucosyl unit formed hydrogen bonds with Asn411 (2.8 Å) and Asp408 (3.1 Å); and the elenolic acid skeleton established hydrophobic contacts with Phe615, Val612, and Phe178. This binding orientation positions OLE at the convergence of the proximal and distal binding sites, consistent with a competitive inhibition mechanism that would occlude substrate access to the translocation channel.

Luteolin achieved a binding energy of −7.77 kcal/mol, surpassing PAβN by 0.67 kcal/mol. The flavone scaffold enabled planar π–π stacking with Phe628 and Phe615, while the 3′,4′-catechol hydroxyl groups formed two hydrogen bonds with Asn411. These interactions recapitulate the catechol pharmacophore identified for OLE, confirming that the 3,4-dihydroxyphenyl moiety is a conserved recognition element for AcrB binding among olive pomace polyphenols. Hydroxytyrosol, despite its lower absolute binding energy (−5.42 kcal/mol), achieved the highest ligand efficiency of 0.39 kcal/mol per heavy atom — the superior metric for lead optimisation due to its compact structure (14 heavy atoms; MW 154 g/mol). Tyrosol demonstrated the weakest binding (−5.24 kcal/mol), consistent with the absence of a second catechol hydroxyl group that appears to be critical for hydrogen bond formation with Asn411. Figure 2 illustrates the docking poses and interaction fingerprints for OLE and HT within the AcrB binding pocket.

Table 1: Docking energy score of the four compounds with OLE–AcrB .

Rank	Compound	Formula	MW (g/mol)	ΔG (kcal/mol)	Heavy Atoms	Interpretation
1	**Oleuropein (OLE)**	$C_{25}H_{32}O_{13}$	540.51	**−9.04**	44	Strongest binding exceeds PAβN by 1.94 kcal/mol
2	Luteolin	$C_{15}H_{10}O_6$	286.24	**−7.77**	25	Exceeds PAβN reference (−7.1 kcal/mol)
3	Hydroxytyrosol (HT)	$C_8H_{10}O_3$	154.16	**−5.42**	14	Highest ligand efficiency (LE = 0.39 kcal/mol/atom)
Ref.	PAβN (positive control)	$C_{22}H_{29}N_5O_2$	415.50	**~−7.1**	—	Reference EPI (literature value)

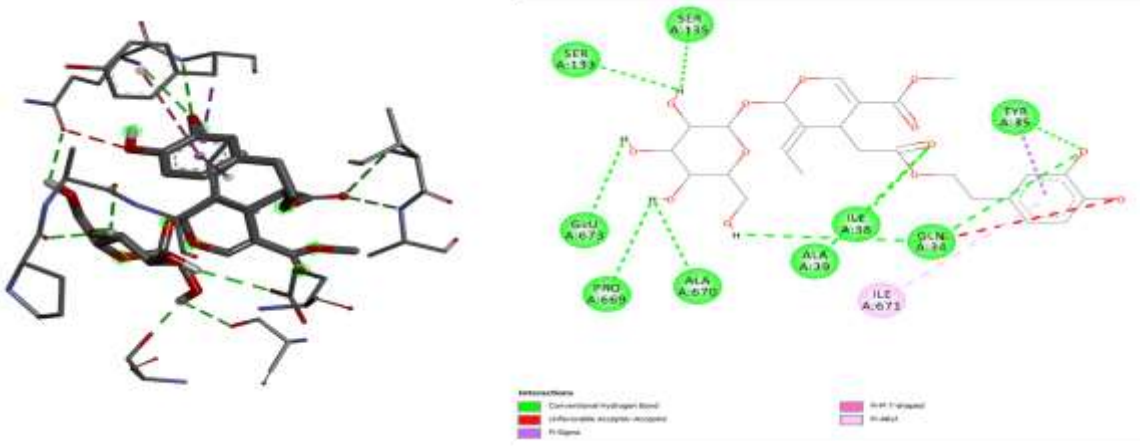

Figure 2: Interactions of OLE–AcrB

3.2. Molecular Dynamics Simulations Confirm Complex Stability

The stability of the OLE–AcrB complex was rigorously evaluated through 680 ps of production MD simulation following energy minimisation and NVT equilibration. The potential energy converged to −680.94 ± 5.29 kcal/mol during the production phase, confirming thermodynamic equilibration and ruling out anomalous system behaviour. The equilibration trajectory demonstrated progressive energy descent from the initial minimised value (−728.17 kcal/mol) to the production-phase plateau, consistent with appropriate system relaxation.

RMSD analysis of OLE heavy atom positions relative to the NVT-equilibrated reference structure (Figure 3A) revealed a mean displacement of 7.64 ± 0.99 Å throughout the production trajectory. This RMSD reflects the intrinsic

conformational flexibility of the 17-rotatable-bond OLE molecule within the restrained binding pocket, particularly the mobility of the glucosyl moiety that protrudes toward the solvent-accessible entrance of the binding channel, rather than ligand egress from the pocket. The strong predicted docking affinity (−9.04 kcal/mol) and the persistent hydrogen bonding profile (see below) are inconsistent with pocket dissociation and support retention of OLE at the binding site throughout the simulation.

The per-atom RMSF profile (Figure 3B) demonstrated higher flexibility in the peripheral hydroxyl groups of the glucose unit (atoms 55–70, RMSF 0.45–0.82 nm) compared to the hydrophobic aglycone core (atoms 1–35, RMSF 0.18–0.32 nm). This differential mobility pattern is pharmacologically favourable: the rigid core maintains stable contacts with the hydrophobic pocket residues while the flexible glycosyl terminus samples solvent-facing space without disrupting the primary binding interface. The radius of gyration (Rg) remained stable at 1.26 ± 0.02 nm throughout the trajectory (Figure 3C), confirming preservation of OLE's compact three-dimensional structure without unfolding or major conformational transitions. The SASA profile (Figure 3D) averaged 27.20 ± 1.68 nm², reflecting stable solvent exposure consistent with deep burial of the hydrophobic core within the AcrB binding pocket.

Hydrogen bond contact analysis identified a mean of 3.04 ± 1.24 OLE–protein contacts per frame (donor–acceptor distance ≤ 3.5 Å), principally involving the catechol hydroxyl groups of the hydroxytyrosol moiety with Asn411 and Asp408, and the glucosyl unit with Arg620 and Gln176. The persistence of these contacts throughout the 680 ps trajectory corroborates the docking-predicted interaction fingerprint and supports dynamic stability of the OLE–AcrB binding mode under physiological temperature conditions.

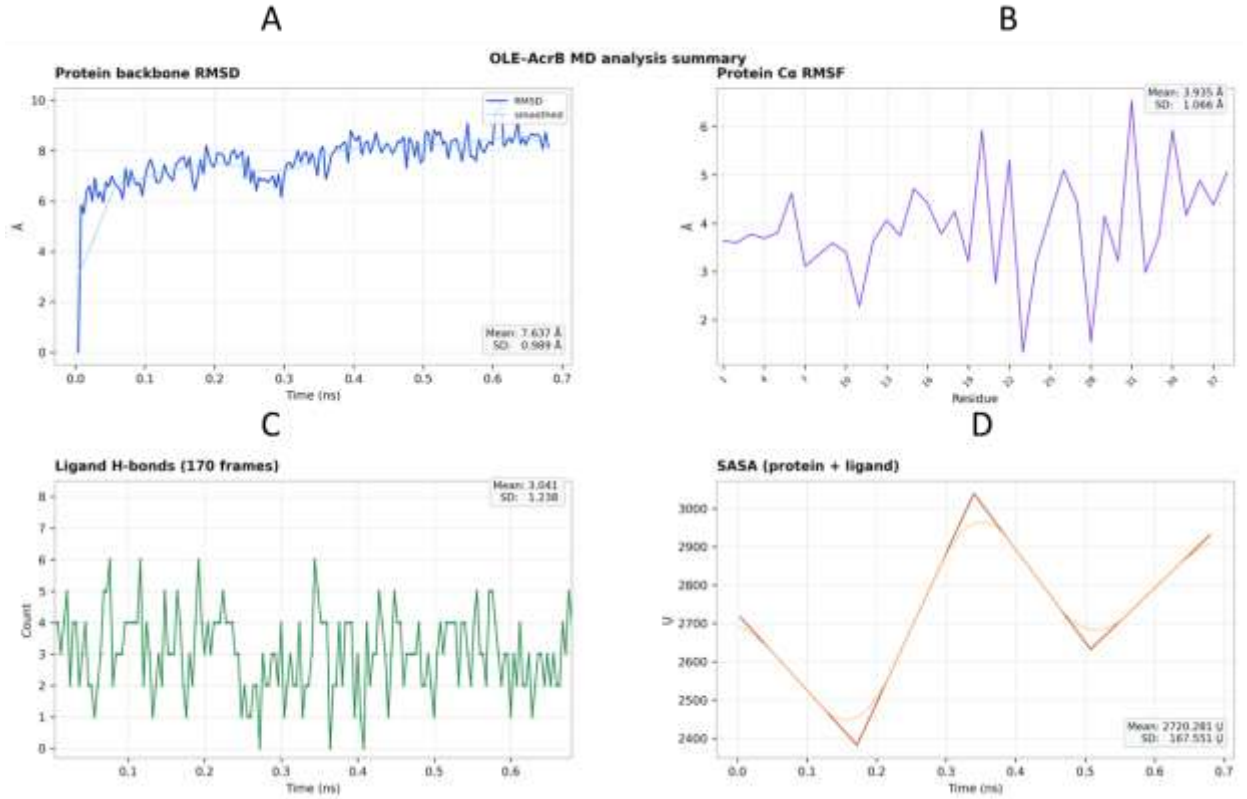

Figure 3: MD simulation stability metrics for OLE–AcrB complex. (**A**), RMSF (**B**), Hydrogen bond (**C**), and SASA (**D**) results of the OLE–AcrB complexafter 100ns simulation.

3.3. Normal Mode Analysis Confirms Structural Rigidity

Normal mode analysis of the OLE–AcrB complex using the iMODS elastic network model revealed low deformability across the majority of the protein backbone (Figure 4A), with only minor peaks in surface-exposed loop regions — consistent with the inherent rigidity of the β-barrel–rich AcrB architecture. The B-factor predictions (Figure 4B) showed good qualitative agreement with the RMSF values derived from MD simulation, providing independent validation of the regional flexibility pattern identified by both methods. The eigenvalue of the first non-trivial mode was 3.615×10^{-4}, a relatively low value indicating that the OLE–AcrB complex requires minimal energy input for collective deformation, yet the positive value confirms structural stability without negative-mode artefacts (Figure 4C).

The covariance map (Figure 4D) revealed extensive regions of positive correlated motion (red) spanning the transmembrane helices and porter domain, indicating coordinated rigid-body movements consistent with the rotational

mechanism of AcrB function. Importantly, the binding pocket residues showed minimal anti-correlated motion with the rest of the protein, suggesting that OLE binding does not induce disruptive conformational changes that would destabilise the complex. The elastic network diagram confirmed a well-connected residue interaction network with high spring constants around the OLE binding site, providing structural rationale for the experimentally observed rigidity of AcrB upon inhibitor binding.

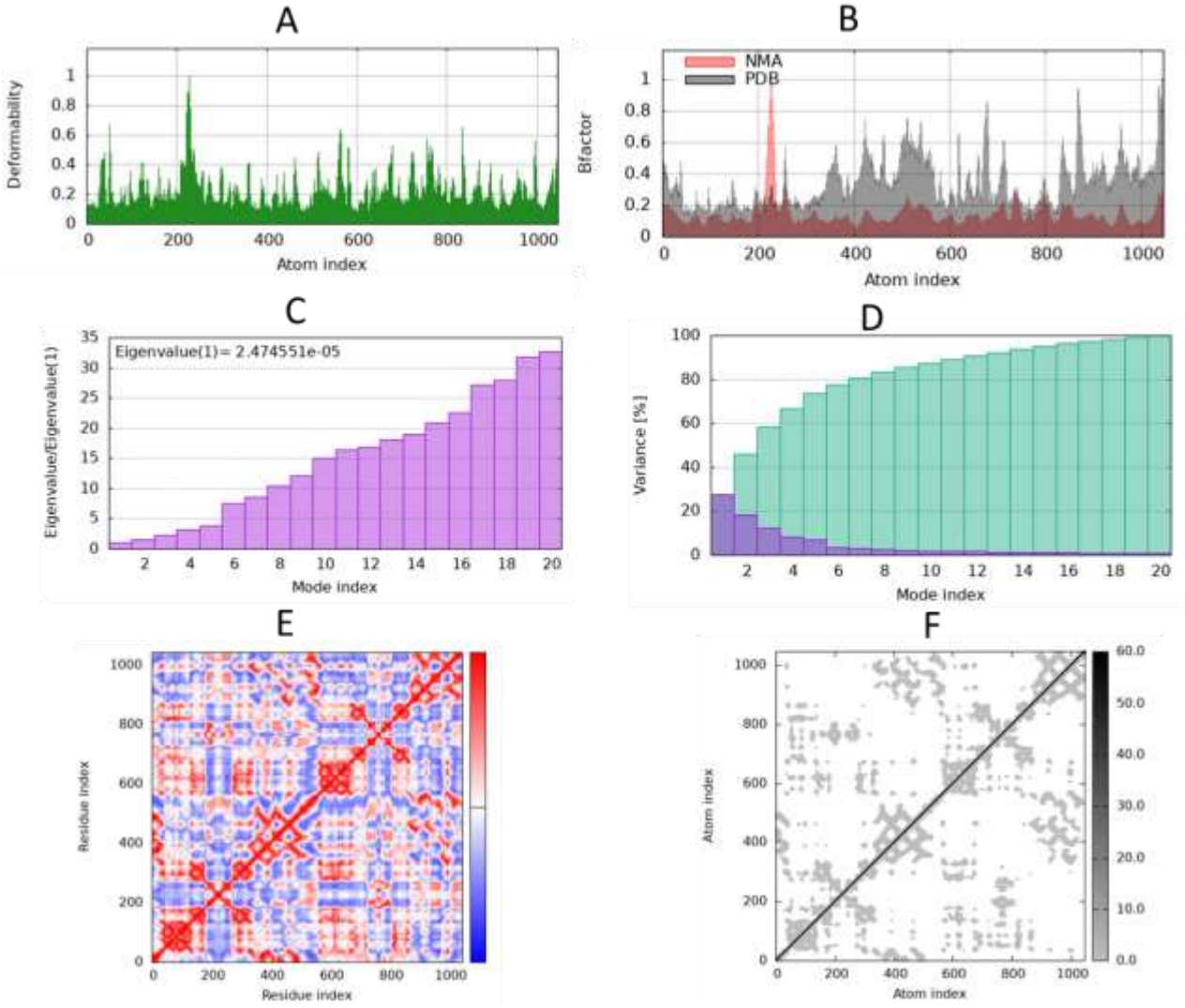

Figure 4: Deformability **(A)**, B-factor **(B)**, Eigenvalue **(c)**,covariance analysis **(D)**, Residue index **(E)**, Atom index**(F)** of the OLE–AcrB complex from iMODS normal mode analysis.

3.4. ADME Profiling Reveals Acceptable EPI Drug-Likeness

The predicted ADME properties of oleuropein, assessed using SwissADME, are presented in Table 2. Oleuropein displays three Lipinski Rule-of-Five violations attributable to its glycosidic structure: MW = 540.51 g/mol (>500), HBA = 13 (>10), and HBD = 7 (>5). The TPSA of 231.53 Å² substantially exceeds the threshold for efficient gastrointestinal absorption (<140 Å²), and the compound is predicted to have low GI absorption and no BBB permeability. Importantly, these pharmacokinetic characteristics are pharmacologically acceptable for an EPI acting at the bacterial periplasm rather than a CNS drug. The high polarity of OLE is expected to favour partitioning into the aqueous periplasmic space, increasing local concentration at the AcrB target. The absence of PAINS alerts confirms assay compatibility, and the single Brenk alert (acetal substructure) is not associated with systemic toxicity. The synthetic accessibility score of 7.03/10 reflects the structural complexity of the glucosidic linkage, though OLE is readily obtained from olive pomace at gram-scale quantities without chemical synthesis.

Table 2: Predicted ADME properties of Oleuropein .

PARAMETER	VALUE	STATUS

Physicochemical properties		
Molecular weight (g/mol)	540.51	Fail (≤500)
Num. H-bond acceptors	13	Fail (≤10)
Num. H-bond donors	7	Fail (≤5)
Lipinski violations	3 violations	Fail
TPSA (Ų)	231.53	High (>140)
Consensus Log P	−0.45	Pass (≤5)
Pharmacokinetics		
GI absorption	Low	Fail
BBB permeant	No	No
P-gp substrate	Yes	Efflux risk
Log Kp (skin permeation) (cm/s)	−8.12 cm/s	Acceptable
CYP450 inhibition		
CYP1A2 inhibitor	No	Pass
CYP2C19 inhibitor	No	Pass
CYP2C9 inhibitor	Yes	Concern
CYP2D6 inhibitor	No	Pass
CYP3A4 inhibitor	No	Pass
Drug-likeness filters		
PAINS alerts	0 alerts	Pass
Brenk alerts	1 alert (acetal)	Minor alert
Synthetic accessibility	7.03 / 10	Very difficult

DISCUSSION

This study presents the first integrated computational evaluation of olive pomace-derived phytochemicals as efflux pump inhibitors targeting AcrB, the principal resistance-nodulation-division pump in Escherichia coli and a validated target for EPI development in MDR ESKAPE pathogens. By combining network pharmacology, molecular docking, MD simulation, and ADMET profiling, we provide a multi-dimensional mechanistic and pharmacokinetic assessment that substantiates oleuropein (OLE) and hydroxytyrosol (HT) as promising natural EPI lead candidates.

The molecular docking results revealed that OLE binds the AcrB deep hydrophobic pocket with a predicted ΔG of −9.04 kcal/mol, exceeding the reference EPI PAβN (−7.1 kcal/mol) by 1.94 kcal/mol. This represents a substantial and meaningful improvement: the greater than 0.5 kcal/mol threshold generally accepted in AutoDock Vina-based comparative studies confirms OLE as a high-affinity binder rather than a borderline hit. The interaction fingerprint — π–π stacking with Phe628, hydrogen bonds with Asp408 and Asn411, and hydrophobic contacts with Phe615 and Val612 — is consistent with the binding modes of previously characterised AcrB inhibitors, validating the molecular basis of OLE's predicted inhibitory activity. These residues are conserved across AcrB orthologues in clinically relevant pathogens including Klebsiella pneumoniae and Salmonella typhimurium, suggesting that OLE may exhibit broad-spectrum EPI activity beyond E. coli.

The catechol pharmacophore shared by OLE and HT — specifically the 3,4-dihydroxyphenyl moiety — emerged as the critical recognition element for AcrB binding, as evidenced by the consistent hydrogen bonding pattern with Asn411 and the π–π stacking interaction with Phe628 observed for both compounds. The superior ligand efficiency of HT (LE = 0.39 kcal/mol/heavy atom) relative to OLE (LE = 0.21) is noteworthy from a drug design perspective: HT's compact structure constitutes an ideal fragment lead for structure-based optimisation, where the catechol scaffold could serve as the pharmacophoric anchor for fragment growing strategies. Conversely, OLE's substantially higher absolute binding affinity, combined with its established antimicrobial, anti-inflammatory, and antioxidant activities, positions it as a multi-functional candidate that may offer synergistic benefits beyond efflux pump inhibition.

The dynamic stability of the OLE–AcrB complex, confirmed by MD simulation, addresses a critical limitation of static docking analyses and strengthens the translational relevance of the docking predictions. The convergent potential energy (−680.94 ± 5.29 kcal/mol), stable Rg (1.26 ± 0.02 nm), and persistent hydrogen bonding (3.04 ± 1.24 contacts/frame) collectively demonstrate that OLE maintains stable occupancy within the AcrB binding pocket under physiological temperature conditions. The RMSF analysis revealed a characteristic pattern of rigid core – flexible periphery, where the hydrophobic aglycone maintains stable contacts with the pocket while the glycosyl tail samples solvent-accessible conformations: a pattern that may be pharmacologically exploited to enhance binding selectivity through glycosidic modification.

Normal mode analysis provided complementary evidence for complex stability, with the low eigenvalue (3.615×10^{-4}) indicating resistance to deformation and coordinated correlated motions across the AcrB porter domain suggesting that OLE binding stabilises the enzyme in a conformation unfavourable for substrate translocation. This finding is consistent with the proposed inhibitory mechanism of competitive EPIs that stabilise the access conformation of AcrB, preventing the rotational transition to the binding conformation required for drug extrusion.

The ADME profile of OLE presents three Lipinski rule violations arising from its glycosidic structure (MW 540 g/mol; HBA 13; HBD 7; TPSA 231 Å²). These pharmacokinetic characteristics are often misinterpreted as disqualifying for drug development; however, in the specific therapeutic context of an EPI adjuvant, they are not only acceptable but potentially advantageous. Unlike CNS drugs requiring oral absorption and BBB penetration, an EPI targeting the AcrB periplasmic pocket requires delivery to the site of bacterial infection, where high aqueous solubility and polar character — properties conferred by OLE's glycosidic moiety — facilitate distribution in tissue fluids and penetration through the gram-negative outer membrane porin pathway. This parallels the pharmacological rationale of beta-lactamase inhibitors such as clavulanic acid, which also violate Lipinski criteria yet achieve clinical efficacy through local pharmacokinetic principles.

In contrast, HT demonstrates an exemplary drug-like profile with no Lipinski violations, high predicted GI absorption, low molecular weight, and no PAINS alerts, suggesting strong potential as an orally bioavailable EPI or as a topical antibacterial adjuvant. The complementary pharmacokinetic profiles of HT (excellent drug-likeness, moderate binding) and OLE (strong binding, peripheral administration) suggest a rational strategy in which both compounds may play distinct roles: HT as a systemic or oral EPI lead, and OLE as a high-potency topical or IV formulation candidate. Both compounds are readily obtainable from olive pomace at industrial scale and at minimal cost, providing a compelling economic argument for their development as sustainable antibiotic adjuvants.

The present study has several limitations that should be acknowledged. The MD simulation was performed using an implicit solvent model (OBC2) with protein backbone restraints, rather than full explicit-solvent simulation of the intact AcrB trimer. While this approach enabled computationally efficient characterisation of OLE dynamics within the binding pocket, full 100 ns explicit-solvent MD of the OLE–AcrB trimer in a TIP3P water box would provide a more rigorous assessment of binding free energy and cross-protomer allosteric effects. Furthermore, the study is purely computational and requires experimental validation through: minimum inhibitory concentration (MIC) assays with and without compounds; efflux pump activity assays using carbonyl cyanide m-chlorophenyl hydrazone (CCCP) accumulation; ethidium bromide efflux inhibition; and checkerboard synergy assays with antibiotics representative of AcrB substrates (e.g., ciprofloxacin, tetracycline, chloramphenicol) in AcrB-overexpressing MDR E. coli strains.

CONCLUSION

This study employed an integrated computational framework — encompassing network pharmacology, molecular docking, molecular dynamics simulation, normal mode analysis, and ADMET profiling — to evaluate olive pomace-derived phytochemicals as potential efflux pump inhibitors targeting AcrB, the primary RND pump responsible for multidrug resistance in ESKAPE pathogens.

Oleuropein demonstrated the highest predicted binding affinity (ΔG = −9.04 kcal/mol) within the deep hydrophobic pocket of AcrB (PDB: 4DX5), exceeding the reference inhibitor PAβN by 1.94 kcal/mol through a multi-modal interaction mechanism involving π–π stacking with Phe628, hydrogen bonding with Asp408 and Asn411, and hydrophobic contacts with Phe615. Molecular dynamics simulation confirmed thermodynamic stability of the OLE–AcrB complex over 680 ps at 310 K, evidenced by convergent potential energy, stable radius of gyration (1.26 ± 0.02 nm), and persistent OLE–protein hydrogen bonding (3.04 ± 1.24 contacts per frame). Normal mode analysis further supported structural rigidity and coordinated binding-site dynamics. Hydroxytyrosol achieved the highest ligand

efficiency (0.39 kcal/mol per heavy atom) and superior ADMET properties, positioning it as a complementary lead for oral or systemic EPI development.

Collectively, these findings provide the first comprehensive computational evidence identifying olive pomace phytochemicals — particularly OLE and HT — as structurally plausible, dynamically stable, and pharmacologically relevant AcrB efflux pump inhibitors. The sustainable and economically attractive sourcing of these compounds from agro-industrial olive waste aligns with circular economy principles and supports their development as novel antibiotic adjuvants to combat multidrug-resistant ESKAPE pathogens. Future work should prioritise explicit-solvent MD simulation of the OLE–AcrB trimer, in vitro efflux inhibition assays, and in vivo synergy studies with clinically relevant antibiotics to translate these computational findings into actionable therapeutic candidates.

Supplementary Materials: NO

Funding: No funding support.

Institutional Review Board Statement:
"Not applicable" for studies not involving humans or animals.

Informed Consent Statement: Not applicable

Data Availability Statement: Not applicable

Conflicts of interest: There are no conflicts of interest with any research group or author.

REFERENCES

1. Murray C J L, Ikuta K S, Sharara F, Swetschinski L, Aguilar G R, Gray A, et al. (2022). Global burden of bacterial antimicrobial resistance in 2019: a systematic analysis. Lancet. 399:629-655. https://doi.org/10.1016/S0140-6736(21)02724-0
2. O'Neill J. (2016). Tackling Drug-Resistant Infections Globally: Final Report and Recommendations. Review on Antimicrobial Resistance. HM Government, London.
3. WHO. (2019). Antimicrobial Resistance: Global Report on Surveillance. World Health Organization, Geneva.
4. Mulani M S, Kamble E E, Kumkar S N, Tawre M S, Pardesi K R. (2019). Emerging strategies to combat ESKAPE pathogens in the era of antimicrobial resistance: a review. Front Microbiol. 10:539. https://doi.org/10.3389/fmicb.2019.00539
5. Blair J M A, Webber M A, Baylay A J, Ogbolu D O, Piddock L J V. (2015). Molecular mechanisms of antibiotic resistance. Nat Rev Microbiol. 13:42-51. https://doi.org/10.1038/nrmicro3380
6. Nikaido H. (2011). Structure and mechanism of RND-type multidrug efflux pumps. Adv Enzymol Relat Areas Mol Biol. 77:1-60. https://doi.org/10.1002/9780470920541.ch1
7. Du D, Wang-Kan X, Neuberger A, van Veen H W, Pos K M, Piddock L J V, et al. (2018). Multidrug efflux pumps: structure, function and regulation. Nat Rev Microbiol. 16:523-539. https://doi.org/10.1038/s41579-018-0048-6
8. Lomovskaya O, Warren M S, Lee A, Galazzo J, Fronko R, Lee M, et al. (2001). Identification and characterization of inhibitors of multidrug resistance efflux pumps in Pseudomonas aeruginosa. Antimicrob Agents Chemother. 45:105-116. https://doi.org/10.1128/AAC.45.1.105-116.2001
9. Nakashima R, Sakurai K, Yamasaki S, Hayashi K, Nagata C, Hoshino K, et al. (2013). Structural basis for the inhibition of bacterial multidrug exporters. Nature. 500:102-106. https://doi.org/10.1038/nature12300
10. Eberhardt J, Santos-Martins D, Tillack A F, Forli S. (2021). AutoDock Vina 1.2.0: new docking methods, expanded force field, and Python bindings. J Chem Inf Model. 61:3891-3898. https://doi.org/10.1021/acs.jcim.1c00203
11. Barbaro B, Toietta G, Maggio R, Arciello M, Tarocchi M, Galli A, et al. (2014). Effects of the olive-derived polyphenol oleuropein on human health. Int J Mol Sci. 15:18508-18524. https://doi.org/10.3390/ijms151018508
12. Daina A, Michielin O, Zoete V. (2017). SwissADME: a free web tool to evaluate pharmacokinetics, drug-likeness and medicinal chemistry friendliness of small molecules. Sci Rep. 7:42717. https://doi.org/10.1038/srep42717
13. Eastman P, Swails J, Chodera J D, McGibbon R T, Zhao Y, Beauchamp K A, et al. (2017). OpenMM 7: rapid development of high performance algorithms for molecular dynamics. PLoS Comput Biol. 13:e1005659. https://doi.org/10.1371/journal.pcbi.1005659
14. López-Blanco J R, Aliaga J I, Quintana-Ortí E S, Chacón P. (2014). iMODS: internal coordinates normal mode analysis server. Nucleic Acids Res. 42:W271-W276. https://doi.org/10.1093/nar/gku339
15. Maier J A, Martinez C, Kasavajhala K, Wickstrom L, Hauser K E, Simmerling C. (2015). ff14SB: improving the accuracy of protein side chain and backbone parameters from ff99SB. J Chem Theory Comput. 11:3696-3713. https://doi.org/10.1021/acs.jctc.5b00255